Drury, K. (1978) *Differentiation (Berlin) 10*, 181–186.
Gerhart, J., Wu, M., & Kirschner, M. (1984) *J. Cell Biol. 98*, 1247–1255.
Guerrier, P., & Doree, M. (1975) *Dev. Biol. 47*, 341–348.
Guerrier, P., Moreau, M., & Doree, M. (1977) *Mol. Cell. Endocrinol. 7*, 137–150.
Gurley, L. R., Walters, R. A., & Tobey, R. A. (1974) *J. Cell Biol. 60*, 356–364.
Hermann, J., Belle, R., Tso, J., & Ozon, R. (1983) *Cell Differ. 13*, 143–148.
Hermann, J., Mulner, O., Belle, R., Marot, J., Tso, J., & Ozon, R. (1984) *Proc. Natl. Acad. Sci. U.S.A. 81*, 5150–5154.
Kanatani, H., & Nagahama, Y. (1980) *Biomed. Res. 1*, 273–291.
Kishimoto, T., & Kanatani, H. (1973) *Exp. Cell Res. 82*, 296–302.
Kishimoto, T., Yoshikuni, M., Ikadai, H., & Kanatani, H. (1985) *Dev., Growth Differ. 27*, 233–242.
Lake, R. S. (1973) *J. Cell Biol. 58*, 317–331.
Langan, T. A. (1978) *Methods Cell Biol. 19*, 143–152.
LeGoascogne, C., Sananes, N., Gouezou, M., & Baulieu, E. E. (1984) *C. R. Acad. Sci., Ser. 3 299*, 89–93.
Maller, J. L. (1985) *Cell Differ. 16*, 211–221.
Maller, J., Wu, M., & Gerhart, J. C. (1977) *Dev. Biol. 58*, 295–312.
Masui, Y., & Clarke, H. J. (1979) *Int. Rev. Cytol. 57*, 185–282.
Meijer, L., & Guerrier, P. (1984) *Int. Rev. Cytol. 86*, 129–196.
Meijer, L., & Zarutskie, P. (1987) *Dev. Biol. 121*, 306–315.
Meijer, L., Guerrier, P., & Maclouf, J. (1984) *Dev. Biol. 106*, 368–378.
Meijer, L., Brash, A. R., Bryant, R. W., Ng, K., Maclouf, J., & Sprecher, H. (1986a) *J. Biol. Chem. 261*, 17040–17047.
Meijer, L., Pondaven, P., Tung, H. Y. L., Cohen, P., & Wallace, R. W. (1986b) *Exp. Cell Res. 163*, 489–499.
Nemoto, S. I. (1982) *Dev., Growth Differ. 24*, 429–442.
Pelech, S. L., & Krebs, E. G. (1987) *J. Biol. Chem. 262*, 11598–11606.
Pelech, S. L., Meijer, L., & Krebs, E. G. (1987) *Biochemistry* (preceding paper in this issue).
Picard, A., Peaucellier, G., Le Bouffant, F., Le Peuch, C., & Doree, M. (1985) *Dev. Biol. 109*, 311–320.
Picard, A., Labbe, J. C., Peaucellier, G., Le Bouffant, F., Le Peuch, C., & Doree, M. (1987) *Dev., Growth Differ. 29*, 93–103.
Pondaven, P., & Meijer, L. (1986) *Exp. Cell Res. 163*, 477–488.
Quirin-Stricker, C. (1984) *Eur. J. Biochem. 142*, 317–322.
Sano, K. (1985) *Dev., Growth Differ. 27*, 263–275.
Scott, J. D., Glaccum, M. B., Fischer, E. H., & Krebs, E. G. (1986) *Proc. Natl. Acad. Sci. U.S.A. 83*, 1613–1616.
Woodford, T. A., & Pardee, A. B. (1986) *J. Biol. Chem. 261*, 4669–4676.
Wu, M., & Gerhart, J. C. (1980) *Dev. Biol. 79*, 465–477.
Wu, R. S., Panusz, H. T., Hatch, C. L., & Bonner, W. M. (1986) *CRC Crit. Rev. Biochem. 20*, 201–263.

Two-Dimensional Crystals of Enzyme–Effector Complexes: Ribonucleotide Reductase at 18-Å Resolution†

Hans O. Ribi,‡ Peter Reichard,§ and Roger D. Kornberg*,‡

Department of Cell Biology, Stanford University School of Medicine, Stanford, California 94305, and Medical Nobel Institute, Department of Biochemistry, Karolinska Institute, S-104 01 Stockholm, Sweden

Received March 11, 1987; Revised Manuscript Received June 18, 1987

ABSTRACT: The B1 subunit of ribonucleotide reductase formed two-dimensional crystals when bound to an effector nucleotide linked to lipids in planar layers at the air/water interface. The effector lipid consisted of dATP coupled through the γ-phosphoryl group and an ε-aminocaproyl linker to phosphatidylethanolamine. Two-dimensional crystals of B1 reductase, like those of antibodies and cholera toxin obtained previously, formed under physiologic conditions of pH and ionic strength, with no precipitant added to the solution. There was, however, a requirement for dTTP in the solution, presumably to ensure binding of the dATP–lipid at only one of two effector sites on the enzyme. Diffraction from the crystals extended to 18-Å resolution in negative stain, with unit cell parameters a = 110 Å, b = 277 Å, and γ = 90°. Image analysis revealed the B1 dimer as a pair of roughly cylindrical objects, each 105–109 Å in length and 31–34 Å in diameter.

Ribonucleoside-diphosphate reductase is an enzyme of broad regulatory significance, present in both prokaryotes and eukaryotes (Thelander & Reichard, 1979; Martin & Gelfand, 1981; Follman, 1982; Reichard & Ehrenberg, 1983). It catalyzes and controls the reduction of ribonucleoside diphosphates to deoxyribonucleotides and thus partitions nucleotides between RNA and DNA synthesis. The catalytic and regulatory properties of the enzyme derive from the interaction of two types of subunit in a double dimer and from a remarkable set of allosteric effects. In *Escherichia coli*, the dimers are known as B1 (177 000 daltons) and B2 (87 000 daltons) and contain binding sites for effectors (nucleoside triphosphates) and a source of reducing power (dithiols and a stable free radical), respectively. Mechanistic studies have been limited by a lack of structural information. The dimers separate during purification, and single crystals of each dimer have been obtained, but X-ray diffraction analyses have not been completed (Joelson et al., 1984). We report here on imaging the B1 dimer by formation of two-dimensional crystals

† This research was supported by NIH Grants AI21144 and GM30387 to R.D.K. and by a grant from the Swedish Medical Research Council to P.R. H.O.R. received support from Cellular and Molecular Biology Training Grant GM07276-12 from the National Institutes of Health.

* Author to whom correspondence should be addressed.
‡ Stanford University School of Medicine.
§ Karolinska Institute.

0006-2960/87/0426-7974$01.50/0

on lipid layers and electron microscopy.

The lipid layer crystallization technique depends on specific binding of macromolecules to lipid–ligands in planar lipid layers. Binding orients and concentrates the macromolecules in two dimensions, and diffusion of the lipids facilitates crystallization (Uzgiris & Kornberg, 1983; Ribi and Kornberg, unpublished results). This approach has the advantages of rapidity, the requirement for only microgram amounts of material, and the possible extension to molecular complexes. The first application of the technique was to a monoclonal anti-dinitrophenyl-IgG, with *N*-[ϵ-[(2,4-dinitrophenyl)-amino]caproyl]phosphatidylethanolamine as the lipid–ligand. Linear and hexagonal arrays of the IgG formed under a range of solution conditions (Uzgiris & Kornberg, 1983), and electron micrographs gave diffraction extending to about 20-Å resolution (Reidler et al., unpublished results). Recently, the approach was used to study cholera toxin bound to lipid layers containing its natural receptor, the ganglioside GM_1. Rectangular lattices of the toxin and derivatives were obtained under various conditions, and the structures were determined at about 15-Å resolution (Ludwig et al., 1986; Ribi et al., 1987).

In the present study, we synthesized a lipid-linked nucleotide for binding the ribonucleotide reductase B1 dimer to lipid layers. B1 reductase crystals formed under essentially physiologic conditions, indicating that our previous successes with monoclonal IgG and cholera toxin were not due to some peculiarity of antibody structure or natural association of toxin with membranes but rather that the lipid layer crystallization technique may be generally useful for imaging molecular complexes under conditions of interest.

Experimental Procedures

Materials. ϵ-Aminocaproic acid, *tert*-butyl pyrocarbonate (t-BOC), dicyclohexylcarbodiimide (DCC), phospholipase A_2 (*Crotalus durissus*), and silica gel (250 mesh) were from Sigma. Thin-layer chromatography (TLC) plates and preparative TLC plates (E. Merck Darmstadt) were from American Scientific Products. L-α-Dioleoylphosphatidylethanolamine (PE) and egg phosphatidylcholine (PC) were from Avanti Polar Lipids, and aminocaproyl-PE was synthesized as described below or purchased from Avanti.

Analysis. The progress of reactions and purity of final products were assessed by TLC on silica gel 60 F254 plates developed with chloroform–methanol–water (10:6:1 v/v). Adenine was revealed by UV quenching, phosphorus with molybdenum blue spray (Dittmer & Lester, 1964), and ^{32}P by autoradiography. Phospholipase A_2 digestion was performed as described (Worthington Enzyme Manual, Worthington Biochemical Corp., Freehold, NJ) with modifications: 0.5 mg of lipid was dried in a glass vial and dispersed by sonication in 100 μL of assay buffer containing 0.0005% Triton X-100. One unit of enzyme was added, and lipid hydrolysis was monitored by extraction with chloroform–methanol (4:1 v/v) and TLC. Phosphorus determination was as described (McClare, 1971). ^1H NMR spectra were recorded with an NMC300 Nicolet spectrometer with $CDCl_3$ and Silanor-C (Merck) as solvents. Liquid secondary ion mass spectra (LSIMS) were taken with an MS-50 mass spectrometer (Mass Spectrometry Resource, University of California, San Francisco, CA).

dATP–Aminocaproyl-PE. t-BOC-aminocaproic acid [93 mg, 4.0×10^{-4} mol, prepared as described (Moroder et al., 1976)] and DCC (167 mg, 8.1×10^{-4} mol) were combined in 1 mL of dry dichloromethane and stirred at room temperature for 40 min. A precipitate of dicyclohexyl urea was removed by filtration through glass wool, and the filtrate was added to 75 mg (1.0×10^{-4} mol) of PE in 1 mL of dry dichloromethane and 150 μL of dry pyridine. The mixture was stirred for 2 h, diluted with 1 volume of acetone, and applied to a column of silica gel. The column was washed with chloroform–acetone (1:1 v/v) and eluted with chloroform–methanol under low pressure (10 psi). The solvent was removed in vacuo yielding 65 mg of t-BOC-aminocaproyl-PE (68% yield based on starting PE). Infrared (KBr pellet): bands at 1660 cm^{-1} (carbonyl) and 3400 cm^{-1} (amide).

The amino-protecting group was removed from 65 mg of t-BOC-aminocaproyl-PE as described (Paltauf, 1976) by bubbling with dry HCl gas in 5 mL of dry chloroform with stirring for 30 min at 0 °C. HCl and solvent were removed in vacuo, and the residue was fractionated on a silica gel column, yielding 31 mg of aminocaproyl-PE (53% yield based on t-BOC-aminocaproyl-PE). Digestion with phospholipase A_2 demonstrated an intact phospholipid by conversion to a lysophospholipid. Infrared (KBr pellet): bands at 3350 and 3210 cm^{-1} (amine). LSIMS. Calcd for $C_{47}H_{89}O_9N_2P$: 856. Found: 856.

dATP was condensed with aminocaproyl-PE as described (Knorre et al., 1976) with modifications. The disodium salt of dATP was adsorbed on DE-52 (Whatman), washed with 10–50 mM triethylammonium bicarbonate, and eluted with 500 mM triethylammonium bicarbonate (pH 7.0). The resulting triethylammonium salt of dATP (72 mg, 10^{-4} mol) and 100 μCi of the triethylammonium salt of [α-^{32}P]dATP (Amersham) were mixed, dried in vacuo, and dissolved in 1.5 mL of chloroform–methanol (4:1 v/v). DCC (38 mg, 1.8×10^{-4} mol) was added, and the mixture was kept for 2 h at room temperature. A precipitate of dicyclohexylurea was removed by filtration through glass wool, and the filtrate was added to 25 mg (2.9×10^{-5} mol) of aminocaproyl-PE, 50 μL of dry diisopropylethylamine, and 0.7 mL of dry chloroform. The mixture was stirred at room temperature for 35 h and then fractionated by preparative TLC, yielding a mixture of two components, each of which contained adenine and ^{32}P. The ratio of adenine to ^{32}P remained constant throughout purification. The major component (R_f 0.2) was resolved from the minor one (R_f 0.3) by silica column chromatography, yielding 12 mg of dATP–aminocaproyl-PE (30% yield based on aminocaproyl-PE). Digestion with phospholipase A_2 demonstrated an intact phospholipid by conversion to a lysophospholipid. ^1H NMR ($CDCl_3$): δ 7.3 (m, 2, aryl-H), 5.3 (m, 4, —CH═CH—), 1.0 (s, 6, CH_3). LSIMS. Calcd for $C_{57}H_{103}N_7O_{20}P_4$: 1329. Found: 1351 (major), 1367 (minor), 1343 (major), 1389 (minor). The LSIMS peaks were interpreted as the monosodium salt (1351) and its lipid peroxidized form (1367) and the disodium salt (1373) and its lipid peroxidized form (1389).

Surface Pressure Measurements. Teflon or glass troughs (3-cm^2 surface area, 1 mm deep) were filled with water or buffer [0.1–0.3 M NaCl, 10 mM tris(hydroxymethyl)-aminomethane hydrochloride (Tris-HCl), pH 7.4, 5 mM $MgCl_2$], and lipids (0.5 mg/mL) in chloroform–hexane (1:1 v/v) were applied to the surface. Lateral pressures were monitored with time by the Wilhelmy plate method (Möbius et al., 1969).

Crystallization and Electron Microscopy. For electron microscopy of single B1 particles, frozen aliquots of B1 reductase [9 mg/mL, prepared as described (Brown et al., 1969)] were thawed and diluted to 10 μg/mL with a buffer containing 100 mM NaCl, 15 mM $MgCl_2$, 5 mM spermidine, and 15 mM Tris-HCl (pH 7.6) at 4 °C. Droplets of protein solution were placed on carbon-coated electron microscope

grids for 2–5 min at room temperature (grids were made hydrophilic by treatment with amylamine and glow discharge). After removal of the majority of the solution by blotting, the grids were washed with 1 drop of distilled water and then stained for 30–60 s with 1% uranyl acetate.

For preparation of rectangular lattices, aliquots of B1 (described above) were diluted to 250 μg/mL with a buffer containing 100 mM NaCl, 5–15 mM $MgCl_2$, 2–10 mM spermidine, 2 mM dTTP, and 15 mM Tris-HCl (pH 7.6) and kept at 4 °C for 0.5–1 h. Droplets of B1 solutions (14 μL) were then placed in Teflon wells (4-mm diameter, 1 mm deep), and the surfaces of the droplets were coated with 0.25–0.5 μL of a lipid mixture containing 7.4×10^{-5} M dATP–aminocaproyl-PE and 5.1×10^{-4} M egg PC (molecular weight based on dioleoyl form, in chloroform–hexane–methanol, 10:10:0.5 v/v), followed by incubation in a humid chamber at room temperature for 24–48 h. Electron microscope grids, freshly coated with carbon, were floated on the wells (carbon facing the solution) for 5 min, withdrawn, washed with 1 drop of distilled water, and then stained for 30–60 s with 1% uranyl acetate. Micrographs were recorded with minimal electron doses (10–15 electrons/Å^2 per image) on a Philips EM 400 operating at 100 kV. Image processing was performed according to standard methods (Amos et al., 1982).

Results

A lipid-linked nucleotide was a natural choice for binding the B1 dimer to lipid layers. There are three nucleotide-binding sites on each B1 polypeptide, one for substrates and two for effectors (Thelander & Reichard, 1979). ATP, dATP, dTTP, and dGTP bind at one effector site ("h site") and modulate the substrate specificity of the enzyme, assuring a balanced distribution of the four deoxynucleotide products. ATP and dATP bind at the other effector site ("l-site"), raising and lowering the overall activity of the enzyme, respectively. We made use of dATP binding in the present studies because the affinity for dATP is the highest at both sites and because binding may be directed to one site or the other (Brown & Reichard, 1969). Alone, dATP shows a 17-fold preference for binding at the h site (dissociation constant of 0.3×10^{-7} M, compared with 5×10^{-7} M at the l site), whereas in the presence of excess dTTP binding occurs exclusively at the l site.

For linkage of dATP to a lipid, the γ-phosphoryl group of the nucleotide was coupled through an ϵ-aminocaproyl linker to dioleoyl-PE. The rationale for this structure is as follows: substituents at the γ-phosphoryl position of dATP do not prevent binding to ribonucleotide reductase (Berglund & Eckstein, 1974); the insertion of a caproyl linker between PE and a dinitrophenyl group was important for binding of polyclonal anti-dinitrophenyl antibodies to lipid vesicles (Six et al., 1973) and for crystallizing a monoclonal antibody (Ribi and Kornberg, unpublished results), presumably to avoid steric hindrance of binding to the lipid layer; and a dioleoyl lipid was used to assure lateral mixing with other unsaturated phospholipids in lipid layers.

Synthesis of dATP–aminocaproyl-PE was carried out in two steps. First, *tert*-butylcarbonyl-ϵ-aminocaproic acid was joined

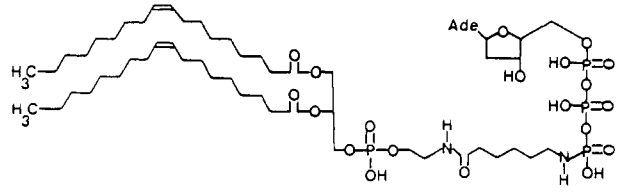

dATP–aminocaproyl-PE

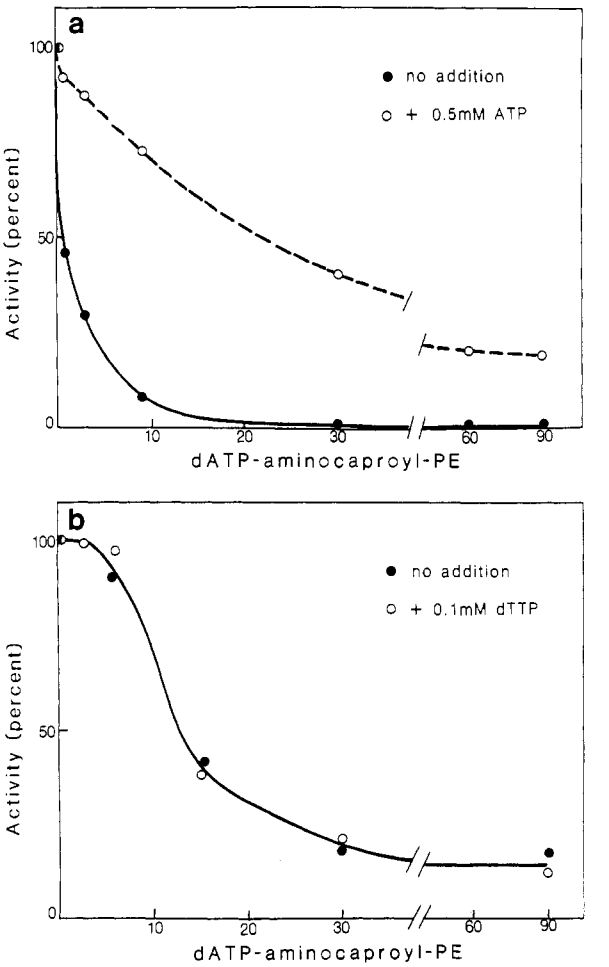

FIGURE 1: Effect of dATP–aminocaproyl-PE on the reduction of CDP by ribonucleotide reductase. In two separate experiments, aqueous dispersions of dATP–aminocaproyl-PE, sonicated until clear, were added in the amounts indicated to reaction mixtures containing all reagents required for optimal reduction of CDP (Brown et al., 1969), with and without ATP (panel a) or dTTP (panel b). Results are expressed as percentage of controls with no addition of dATP–aminocaproyl-PE, corresponding to 10 enzyme units (no ATP) and 18 units (+ATP) in panel a and 1 unit (no dTTP) and 3 units (+dTTP) in panel b.

in an amide linkage to PE and the *tert*-butylcarbonyl group was removed, to form ϵ-aminocaproyl-PE. Second, dATP was coupled to the amino moiety of aminocaproyl-PE in a reaction specific for the γ-phosphoryl group of many nucleoside triphosphates (Knorre et al., 1976). The intermediate, aminocaproyl-PE, may be generally useful in the synthesis of lipid-linked ligands.

Binding of dATP–aminocaproyl-PE to ribonucleotide reductase was demonstrated by the effect on enzyme activity with CDP as substrate. Low concentrations of dATP (0.1–1 μM) stimulate the reaction through binding at the h site, while tenfold higher concentrations are inhibitory due to additional interactions at the l site (Brown & Reichard, 1969). Sonic dispersions of dATP–aminocaproyl-PE gave no stimulation at low concentrations but inhibited the enzyme at higher concentrations (Figure 1). Inhibition can be attributed to binding at the l site, since it was reversed by ATP but not by dTTP. Apparently, dATP–aminocaproyl-PE binds only at the l site or binds simultaneously at both sites, but even at a low concentration it does not bind exclusively at the h site, possibly due to its high local concentration in lipid vesicles or to steric inhibition of binding at the h site.

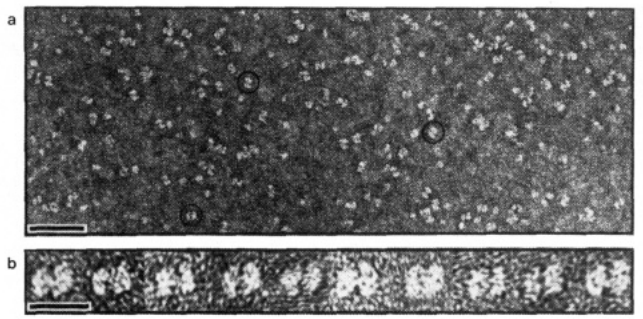

FIGURE 2: Electron micrographs of negatively stained single particles of B1 reductase. (a) B1 randomly adsorbed to a hydrophilic electron microscope grid. Three examples of particles showing a division of protein density into two components are circled. Scale bar, 600 Å. (b) Gallery of individual particles at high magnification. Scale bar, 200 Å.

The formation of lipid layers containing dATP–aminocaproyl-PE was monitored by measuring surface pressures at the air/water interface. Monolayers of pure dATP–aminocaproyl-PE spread on water as described (Gaines, 1966) gave similar pressure–area profiles to dioleoylphosphatidylcholine (dioleoyl-PC), with collapse on compression to about 48 dyn/cm. However, films of dATP–aminocaproyl-PE spread on a fixed surface area over salt solutions (see Experimental Procedures) were unstable, collapsing within minutes of formation. This instability was overcome by adding other lipids. A mixture of egg PC and dATP–aminocaproyl-PE in a 9:1 molar ratio formed monolayers as stable as those of pure egg PC, and films of roughly this composition were used to crystallize the reductase B1 dimer.

In the absence of lipid layers, the B1 dimer adsorbed to electron microscope grids, but no ordered arrays were observed even at high protein concentrations (0.25–1.0 mg/mL), arguing against the formation of arrays in solution prior to the crystallization procedure. At low protein concentrations (10 μg/mL), single particles of B1 were discernible (Figure 2). In the presence of lipids and with dTTP in the solution, three types of ordered arrays of the B1 dimer were obtained, depending on the conditions. Poorly ordered arrays formed at low magnesium concentrations (2–5 mM), during extended incubation (3–9 days) at a reduced temperature (4 °C) (Figure 3a). These arrays appeared multilayered and gave diffuse diffraction extending to only $^1/_{37}$ Å^{-1} (Figure 3b). Parallel rows of filaments formed at high magnesium concentrations (50–100 mM), during 2–3 days at either 4 or 23 °C. The filaments were 143-Å wide, with an axial periodicity of 113 Å (Figure 3c), and when well aligned, gave diffraction extending to about $^1/_{20}$ Å^{-1} (Figure 3d). True two-dimensional crystals formed in the presence of 5–15 mM magnesium and 2–10 mM spermidine, during 1–2 days at room temperature (Figure 4a,b). Diffraction extended to $^1/_{18}$ Å^{-1} (Figure 4c) and revealed a rectangular unit cell with parameters a = 110 ± 3 Å, b = 277 ± 2 Å, and γ = 90° ± 2°. Tilted specimens showed discrete diffraction to a comparable resolution, indicating that the crystals were single layered. A thickness of roughly 33 Å was estimated from views of crystal edges.

When dATP–aminocaproyl-PE was omitted from the lipid layers or when 1.5 mM dATP was added to the solution, there was little protein on the grid and no arrays, showing that specific protein binding was required for success of the procedure. Omission of dTTP caused a marked reduction in array formation. Presumably dTTP prevents dATP–aminocaproyl-PE from binding at a second site on the protein (the h site, see above) and possibly dTTP binding stabilizes the protein. The use of PC, which made up 90% of the lipid layers,

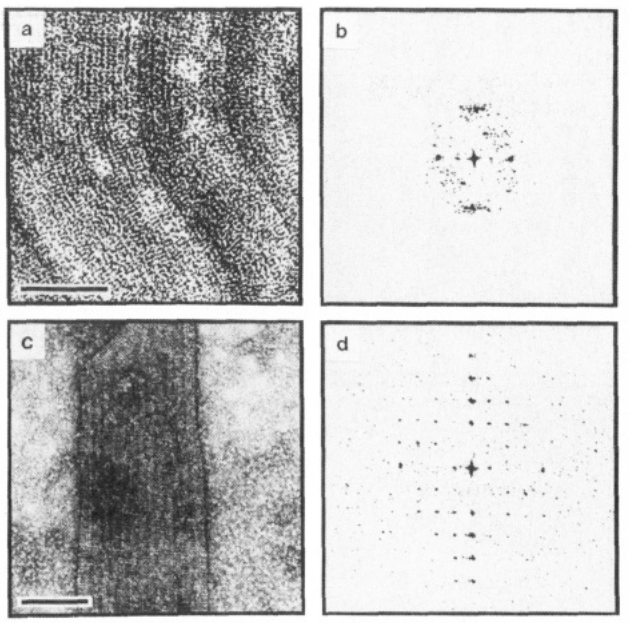

FIGURE 3: Electron micrographs of B1 reductase and two-dimensional arrays in negative stain and corresponding optical diffraction patterns. (a) Arrays formed as described (see Experimental Procedures) except with 5 mM $MgCl_2$, 1–5 mM dithiothreitol, and no spermidine, during 1–14 days at 4 °C. Scale bar, 1000 Å. (b) Optical diffraction pattern of arrays shown in (a). (c) Arrays formed as described except with 50–100 mM $MgCl_2$ and no spermidine at 4 or 23 °C. Scale bar, 1000 Å. (d) Optical diffraction pattern of arrays shown in (c).

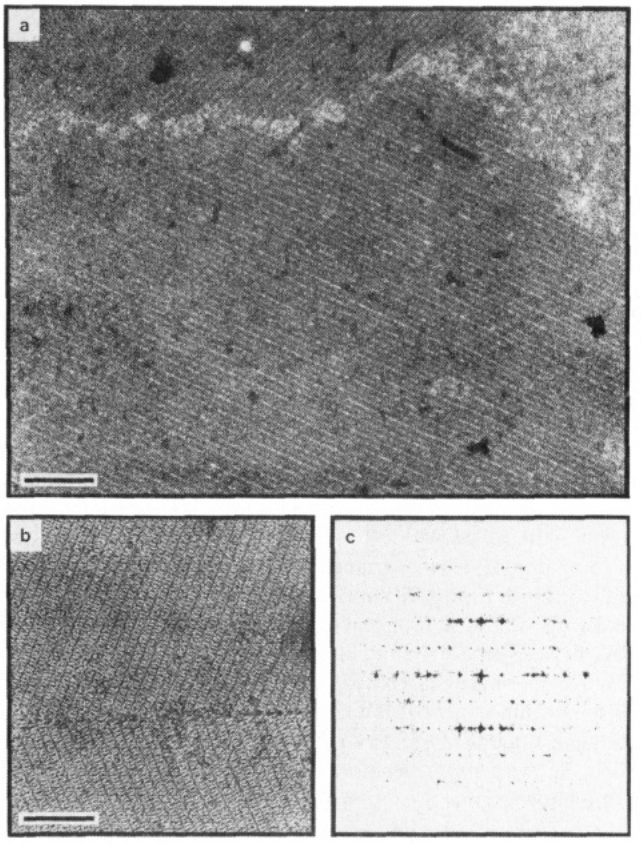

FIGURE 4: Electron micrographs of two-dimensional rectangular crystals of B1 reductase in negative stain (a and b), formed as described under Experimental Procedures, and optical diffraction pattern (c). Scale bars: (a) 1500 Å; (b) 1000 Å.

was also important in the procedure. Substitution of dioleoyl-PE for PC gave protein binding but no ordered arrays. Egg monomethyl- and dimethyl-PE gave arrays, but the degree of

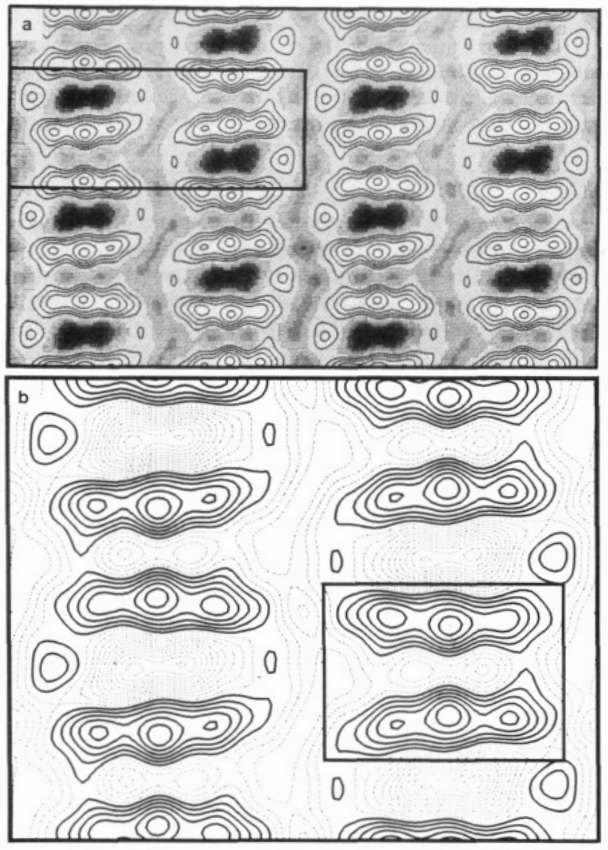

FIGURE 5: Projection map of B1 reductase. (a) Levels of stain are displayed in gray tones, and levels of protein density are indicated by contour lines. The boxed area contains one unit cell [a = 110 Å (vertical direction) and b = 277 Å (horizontal direction)]. Only images of well-stained crystals, as in Figure 3b, were used in the analysis. Crystals lightly embedded in stain, as in Figure 3a, gave processed images with identical pairs of elongated objects, but residual electron density was observed between unit cells along the b direction. (b) A portion of the map in (a), with solid and dashed lines representing positive and negative contours, respectively. The boxed area contains one pair of elongated objects (B1 dimer).

order appeared less than with PC.

Noise-filtered images of the rectangular crystals showed features suggestive of twofold rotational symmetry. On refining the origin of the reciprocal lattice with projected symmetry *p2*, an average difference from centrosymmetric phases of 15° was obtained for seven images. Fourier synthesis with the symmetrized and averaged data gave a density distribution with four elongated objects in the unit cell (Figure 5a, solid contours in boxed area). Each object appeared to be divided in three domains, with a large central peak of density (90 ± 14, in arbitrary units ± standard deviation) flanked by smaller peaks (70 ± 14, average of smaller peaks). The elongated objects were organized in pairs, with strongly staining regions (Figure 5a, darkened areas) between pairs. The long axes of objects within a pair did not lie parallel to each other but rather made an angle of 6°–8° (Figure 5b, boxed region). Imposition of the higher symmetries *c2mm* and *p2gg* would eliminate the angle between the objects, while the remaining possible symmetry *p2mg* would not. *c2mm* symmetry seemed unlikely because the reflection conditions were not satisfied and because of a lack of *mm* symmetry in the diffraction pattern. *p2mg* symmetry was also questionable due to the lack of *mm* symmetry in the diffraction pattern, but deviations from *p2mg* symmetry in the density map (Figure 5) were small. We preferred not to average over this symmetry, since the members of a pair of elongated objects were then independently determined and their similarity provided a measure of the quality of the density map. *p2gg* symmetry was ruled out, because it would not allow the observed alternation of strongly and weakly staining regions between the elongated objects.

Discussion

The image analysis of B1 reductase crystals reported here reveals elongated objects, approximately 105–109 Å in length and 31–34 Å in diameter (contoured at a level where there is contact between objects within a pair). A cylindrical object of these dimensions would have a volume 71–88% of that expected for a B1 monomer (density 1.31 g/cm^3). It therefore seems likely that a pair of objects (boxed in Figure 5b) constitutes a B1 dimer. A test of this interpretation is to calculate the density of protein packing in the unit cell. Two B1 dimers occupy 45% of the unit cell volume (assuming a density of 1.31 g/cm^3 for the protein and a cell thickness of 32.5 Å), which is in the range found for other protein crystals. Further evidence in support of this interpretation comes from electron micrographs of single particles of B1 reductase (Figure 2a). In some particles, a division of the protein density into two equal components could be seen (Figure 2b). The components appeared elongated, with approximate dimensions of 100–110 Å in length and 50–60 Å in diameter. The greater diameter of the components than in the crystals may have resulted from flattening during adsorption to the carbon film and negative staining.

The value of having an image of the B1 dimer from two-dimensional crystals, even at only 18-Å resolution and in projection, is immediately apparent when the image is compared with those of single particles. Electron micrographs of crystals show a consistent division of protein density into elongated units (Figure 4b), whereas this division is only occasionally apparent in images of single particles, presumably due to the variable orientations of the individual particles (Figure 2a). Moreover, the micrographs of crystals are readily analyzed by Fourier methods, giving an averaged, noise-filtered image, whose internal structural details may be discerned. Images from two-dimensional crystals should continue to be useful even after X-ray structures of B1 and B2 subunits have been determined. Decoration of two-dimensional crystals of B1 with B2 subunits may serve as a guide for combining the X-ray structures of the individual subunits to produce a structure of the entire complex. Decoration of two-dimensional crystals can also be used to reveal binding sites of nucleotides (as heavy atom derivatives), monoclonal antibodies, and other interacting molecules.

There are a number of parallels between the present results and those obtained previously with two-dimensional crystals of monoclonal antibodies (Uzgiris & Kornberg, 1983) and cholera toxin (Ludwig et al., 1986; Ribi et al., 1987). In each case more than one type of crystal lattice formed. In all cases, crystallization occurred under physiologic conditions of pH and ionic strength, with no requirement for a precipitant or other unusual component in the solution. There were significant differences in the optimal time of crystallization, temperature, and composition of lipid layers used. The requirement for PC as opposed to PE layers in the case of the B1 dimer was particularly striking. Cholera toxin crystallized equally well with either lipid, whereas antibodies required pure lipid–hapten with no additional phospholipids (Ribi et al., unpublished results). Our success in forming crystals with three different combinations of protein and lipid–ligand, as well as the parallels noted here, points to the generality of the lipid layer crystallization technique. The importance of lipid composition, comparative indifference to solution conditions, and a facile approach for preparing a range of lipid–ligands

provide some guidelines for the application of the technique to other macromolecules.

ACKNOWLEDGMENTS

We thank Drs. P. N. T. Unwin, C. W. Akey, and R. O. Fox for their helpful comments, Dr. E. P. Gogol for the use of his plotting program, and the Mass Spectrometry Resource facility (UCSF) for LSIMS spectra.

Registry No. PE, 4004-05-1; dATP, 1927-31-7; t-BOC-NH-$(CH_2)_5CO_2H$, 6404-29-1; t-BOC-aminocaproyl-PE, 110775-22-9; aminocaproyl-PE, 110796-31-1; dATP–aminocaproyl-PE, 110796-32-2.

REFERENCES

Amos, L. A., Henderson, R., & Unwin, P. N. T. (1982) *Prog. Biophys. Mol. Biol. 39*, 183–231.

Berglund, O., & Eckstein, F. (1974) *Methods Enzymol. 34B*, 253–261.

Brown, N. C., & Reichard, P. (1969) *J. Mol. Biol. 46*, 39–55.

Brown, N. C., Canellakis, Z. N., Lundin, B., Reichard, P., & Thelander, L. (1969) *Eur. J. Biochem. 9*, 561–573.

Dittmer, J. C., & Lester, R. L. (1964) *J. Lipid Res. 5*, 126–127.

Follman, H. (1982) *Naturwissenschaften 69*, 75.

Gaines, G. L., Jr. (1966) *Insoluble Monolayers at Liquid–Gas Interfaces* (Prigogine, I., Ed.) Wiley-Interscience, New York.

Joelson, T., Uhlin, U., Eklund, H., Sjoberg, B.-M., Hahne, S., & Karlsson, M. (1984) *J. Biol. Chem. 259*, 9076–9077.

Knorre, D. G., Kurbatov, V. A., & Samukov, V. V. (1976) *FEBS Lett. 70*, 105–108.

Ludwig, S. D., Ribi, H. O., Schoolnik, G. K., & Kornberg, R. D. (1986) *Proc. Natl. Acad. Sci. U.S.A. 83*, 8585–8588.

Martin, D. W., Jr., & Gelfand, E. W. (1981) *Annu. Rev. Biochem. 50*, 845–877.

McClare, C. N. F. (1971) *Anal. Biochem. 39*, 527–530.

Möbius, D., Bücher, H., Kuhn, H., & Sondermann, J. (1969) *Ber. Bunsen-Ges. Phys. Chem. 73*, 845.

Moroder, L., Hallett, A., Wünsch, E., Keller, O., & Wersin, G. (1976) *Hoppe-Seyler's Z. Physiol. Chem. 357*, 1651–1653.

Paltauf, F. (1976) *Chem. Phys. Lipids 17*, 148–154.

Reichard, P., & Ehrenberg, A. (1983) *Science (Washington, D.C.) 221*, 514–519.

Ribi, H. O., Ludwig, D. S., Mercer, L., Schoolnik, G. K., & Kornberg, R. D. (1987) *Science (Washington, D.C.)* (submitted for publication).

Six, H., Uemura, K., & Kinsky, S. C. (1973) *Biochemistry 12*, 4003–4011.

Thelander, L., & Reichard, P. (1979) *Annu. Rev. Biochem. 48*, 133–158.

Uzgiris, E. E., & Kornberg, R. D. (1983) *Nature (London) 301*, 134–136.

Evidence for the Regulation of Protein Synthesis by a Wheat Germ Phosphoprotein Factor†

Lu Ann Aquino and Mariano Tao*

Department of Biological Chemistry, University of Illinois at Chicago, College of Medicine, Chicago, Illinois 60612

Received June 2, 1987; Revised Manuscript Received July 30, 1987

ABSTRACT: A 48-kilodalton phosphoprotein, termed T-protein or pT, isolated from wheat germ and purified to homogeneity is found to inhibit the translation of tobacco mosaic virus (TMV) RNA in both wheat germ and reticulocyte lysates. The translation of TMV RNA in both systems was inhibited over 80% by 8 μM pT. There was no evidence to indicate that the reticulocyte lysate also contained a pT-like protein. pT was rapidly phosphorylated in the wheat germ and reticulocyte lysates. Although the relationship between pT phosphorylation and inhibition of protein synthesis is not known, there is evidence to indicate that complete phosphorylation of pT is not required for inhibition. Furthermore, no significant differences in the kinetics of inhibition of protein synthesis between prephosphorylated and unmodified pT were observed. Investigation of the mechanism of inhibition indicated that neither the aminoacylation of tRNA nor the elongation of nascent polypeptide chains was affected by pT. On the other hand, pT was found to prevent the formation of the 80S initiation complex. This action of pT was not due to the binding of pT to the ribosomes. However, the effect of pT was found to vary with the concentrations and types of mRNA used in the translational system. These results suggest that pT may interact with specific region(s) of the mRNA and prevent its translation. Alternatively, pT could block the translation of mRNA by binding to one or more of the initiation factors that interact with mRNA to facilitate mRNA binding to the 43S preinitiation complex. On the basis of the action of pT, it is tempting to speculate that this protein could play an important physiological role in contributing to the dormancy of the wheat seed.

Although gene expression in both procaryotes and eucaryotes is controlled to a large extent at the level of transcription, there is increasing evidence also for control at the level of translation. In light of the complexity of the translational process, it is likely that the regulation of translation is also complex, with different mechanisms operating at different steps. Our understanding of the regulation of translation has been derived mainly from studies of the nonnucleated eucaryotic cell reticulocyte [see reviews by de Haro et al. (1985) and Moldave (1985)]. In the reticulocyte, the synthesis of the α and β chains of globin is markedly dependent on the presence

† This work was supported by Grant DK-23045 from the National Institutes of Health.

0006-2960/87/0426-7979$01.50/0